Power gain and dissipation in quantum-dot cellular automata

John Timler and Craig S. Lent[a)]
Department of Electrical Engineering, University of Notre Dame, Notre Dame, Indiana 46556

(Received 18 July 2001; accepted for publication 3 October 2001)

Quantum-dot cellular automata (QCA) may provide a novel way to bypass the transistor paradigm to form molecular-scale computing elements. In the QCA paradigm information is represented by the charge configuration of a QCA cell. We develop a theoretical approach, based on the density matrix formalism, which permits examination of energy flow in QCA devices. Using a simple two-state model to describe the cell, and an energy relaxation time to describe the coupling to the environment, we arrive at an equation of motion well suited to the quasi-adiabatically switched regime. We use this to examine the role of power gain and power dissipation in QCA cells. We show that QCA cells can exhibit true signal power gain. The energy lost to dissipative processes is restored by the clock. We calculate the power dissipated to the environment in QCA circuits and show that it is possible to achieve the ultralow levels of power dissipation required at molecular densities. © *2002 American Institute of Physics.* [DOI: 10.1063/1.1421217]

I. INTRODUCTION

The quantum-dot cellular automata (QCA) concept[1] represents an approach to binary computing which may be more suited to nanoscale implementation than conventional transistors and current switches. A QCA cell represents a bit through the configuration of charge in the cell. As Fig. 1 shows schematically, the cell can be represented as four ''dots,'' which are simply places electrons can occupy. The two charge configurations shown in the figure represent a binary ''1'' and ''0.'' The interaction between cells is purely Coulombic, there is no charge transport between cells. This cell–cell interaction is the basis of QCA device operation.

It should be noted that the QCA computing differs not only from conventional transistor-based designs, but also from analog coherent quantum computing. In QCA information is carried only in classical, not quantum, degrees of freedom, namely in the charge distribution within the cell. Quantum mechanics enables the dynamics of the system; if $\hbar$ were zero, no switching would occur.[2]

The theory of QCA devices and circuits has seen considerable development over the last few years. Binary wires, inverters, and logic gates[3] can be constructed by suitable arrangements of cells (see Fig. 2). The key to larger scale circuit development has been the notion of clocking QCA cells. This entails gradually modulating the interdot barrier so that the cell is unpolarized, put into a ''null'' state, during the switching event. This quasi-adiabatic switching was first proposed by Landauer and Keyes.[4] In the case of QCA, it is the clock signal that modulates the interdot barrier.

Several successful demonstrations of QCA devices have been reported using metal tunnel-junctions in the Coulomb blockade regime. Logic devices, wires, clocked switching, and shift registers have all been demonstrated.[5,6] Architectural studies have led to particular attention being focused on the shift register. QCA can be viewed as a ''processing-in-wire,'' that is, computing while moving information along clocked shift registers.[7]

Implementing QCA cells with single molecules is a new area with considerable promise.[8] Candidate QCA molecules use redox centers in the molecule to play the role of ''dots.'' Appropriate bridging ligands provide a path for tunneling from one dot to another within the molecule.[9] Cell sizes in these systems range from 1 to 5 nm. A specific scheme for clocking molecular cells has been proposed.[10] Molecular QCA represents an approach to the limits of scaling electronics. It also brings into focus fundamental issues regarding power flow in nanoelectronics.

Any successful approach to nanoscale electronics must address two important questions related to energy dissipation.

(1) Do the devices exhibit power gain?
(2) How much power is dissipated?

Question (1) is important because dissipation of signal energy to irreversible loss processes is inevitable. Signal energy lost to such ''frictional'' terms must be replaced. In conventional technology that is done by connections to a power supply. In QCA, we will show that the clock provides the additional energy when it is needed.

Question (2) is crucial because at the phenomenal densities contemplated by molecular electronics, the chip will melt unless each device dissipates only a very small amount of energy to the environment. Adiabatically clocked QCAs offer a means to achieving ultralow power dissipation. The adiabatic theorem[11] guarantees that if the clocking is done slowly enough, any logically reversible process can be implemented with arbitrarily small energy dissipation. Though this settles the question of principle, the practical question remains, at a finite speed how much power is actually dissipated?

The focus of this work is to examine these two issues. The next section develops the formalism we employ to describe clocked QCA cells. Section III uses this formalism to

a)Electronic mail: lent@nd.edu

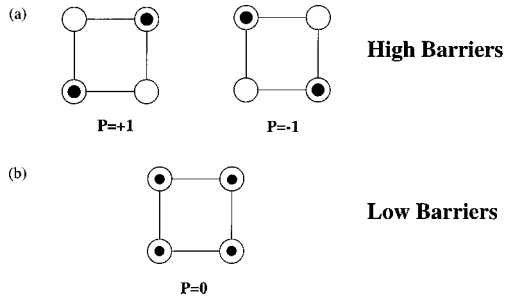

FIG. 1. Schematic of the basic four site cell. (a) When the interdot barriers are high, each electron is essentially localized to a single dot and Coulombic repulsion causes the electrons to occupy antipodal sites within the cell. The two resulting bistable states correspond to cell polarizations of $P=+1$ and $P=-1$. (b) When the interdot barriers are low the electrons are no longer confined to individual dots. The two electron wave function becomes delocalized which results in a cell polarization of $P=0$.

examine a single QCA cell switching. Here we can see deviations from adiabaticity and the resultant dissipation of energy. The basic test-bed for the heart of our work is a QCA shift-register as described in Sec. IV. In Sec. V the formalism for evaluating power flow through the QCA shift-register is developed. Section VI examines the role of power gain in restoring low signals in a shift register. Finally, we evaluate the power dissipated in a QCA shift register as a function of temperature and clocking frequency in Sec. VII.

II. DYNAMICS OF CELLULAR ARRAY

We describe a single QCA cell using a two-state basis composed of the two completely polarized states with polarization $P=+1$ and $P=-1$. The cell polarization in general is then simply $P=-\langle\hat{\sigma}_z\rangle$, the expectation value of the Pauli spin operator.[12] Reference 13 shows how the two-state approximation can be obtained from a more rigorous microscopic Hamiltonian in a well-defined way. For an array of cells we use the intercellular Hartree approximation described in Ref. 13. This entails treating the Coulombic interaction between cells by a mean-field approach. We thereby

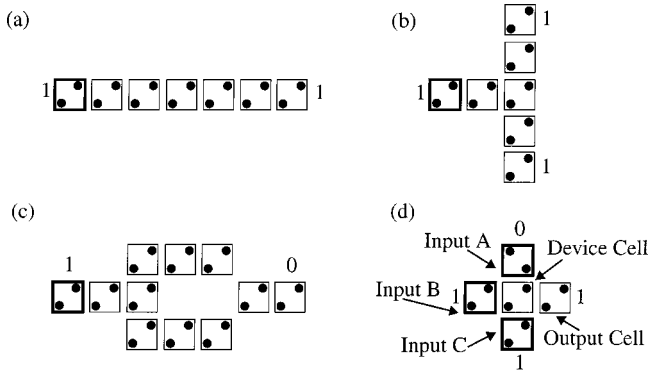

FIG. 2. Fundamental QCA devices: (a) The binary wire transmits data between two points (when clocked it functions as a shift register), (b) fanout provides a method to split a data signal and send the same value to two different destinations, (c) the inverter uses the Coulombic interaction of diagonally aligned cells to invert the input signal, and (d) the majority gate is the fundamental logical element of the QCA architecture where the output is the value corresponding to two or more of the three inputs.

ignore any quantum entanglement between cells. In Ref. 13 the mean-field treatment is quantitatively compared to a fully quantum coherent description of the entire array. For the quasi-adiabatic time evolution considered here, we expect the Hartree approximation to be quite adequate. The Hamiltonian for the jth cell is then

$$\hat{H}_j=\begin{bmatrix} -\frac{E_k}{2}\sum_{m\neq j} f_{j,m}P_m & -\gamma \\ -\gamma & \frac{E_k}{2}\sum_{m\neq j} f_{j,m}P_m \end{bmatrix}. \tag{1}$$

Here $-P_m=\langle\hat{\sigma}_z(m)\rangle$ is the polarization of the mth cell, γ represents the tunneling energy between the two polarization states, and E_k (the so-called ''kink energy'') is an energy which characterizes the Coulombic interaction between cells. Roughly speaking, E_k is the energetic cost of two neighboring cells having opposite polarizations. The term $f_{j,m}$ is a geometrical factor which specifies the interaction between the jth and the mth cells, and can be calculated by a simple application of electrostatics. For the cases of interest here, lines of equally spaced cells, we can absorb the geometric effects into the definition of E_k so that the Hamiltonian can be written

$$\hat{H}_j=\begin{bmatrix} -\frac{E_k}{2}(P_{j-1}+P_{j+1}) & -\gamma \\ -\gamma & \frac{E_k}{2}(P_{j-1}+P_{j+1}) \end{bmatrix}, \tag{2}$$

where we have also ignored next-near-neighbor coupling because the interaction energy between cells decays as the fifth power of the distance. The Hamiltonian for a cell line is just the sum of the Hamiltonians for individual cells.

To include the effects of dissipative coupling to a heat bath we turn to a description based on the density matrix. We employ the coherence vector formalism (also called the generalized Bloch vector)[14] to describe the dynamics of a two state QCA cell connected to an external heat bath. The generators of SU(2), the Pauli spin matrices, form the basis for the coherence vector. The components of the coherence vector ($\vec{\lambda}$) are defined by

$$\lambda_i=\mathrm{Tr}\{\hat{\rho}\hat{\sigma}_i\}. \tag{3}$$

In a similar fashion we project the two-state Hamiltonian onto the basis of generators to form a real three-dimensional energy vector $\vec{\Gamma}$, whose components are

$$\Gamma_i=\frac{\mathrm{Tr}\{\hat{H}\hat{\sigma}_i\}}{\hbar}. \tag{4}$$

The explicit form of the Hamiltonian vector corresponding to Hamiltonian (2) is

$$\vec{\Gamma}=\frac{1}{\hbar}[-2\gamma,0,E_k\overline{P}], \tag{5}$$

where $\overline{P}$ is simply the sum of the neighboring polarizations.

In the absence of coupling to a heat bath, the equation of motion for the two-state coherence vector is

$$\frac{d}{dt}\vec{\lambda} = \vec{\Gamma} \times \vec{\lambda}. \tag{6}$$

This is completely equivalent to the Liouville equation for the density matrix. As shown in Ref. 14, the effect of dissipative coupling, for reasonable assumptions about the bath, is to add an inhomogeneous linear term to this equation, so that it becomes

$$\frac{\partial}{\partial t}\vec{\lambda} = \vec{\Gamma} \times \vec{\lambda} + \xi\vec{\lambda} + \vec{\eta}, \tag{7}$$

with a damping matrix ξ and a damping vector $\vec{\eta}$.

The steady-state density matrix at thermal equilibrium is

$$\hat{\rho}_{ss} = \frac{e^{-\hat{H}/k_B T}}{\mathrm{Tr}\{e^{-\hat{H}/k_B T}\}}. \tag{8}$$

The associated steady-state coherence vector is

$$\vec{\lambda}_{ss} = \mathrm{Tr}\{\hat{\rho}_{ss}\vec{\sigma}\} = -\frac{\hat{\Gamma}}{|\hat{\Gamma}|}\tanh(\Delta), \tag{9}$$

where the temperature ratio (Δ) is defined as

$$\Delta = \frac{\hbar|\vec{\Gamma}|}{2k_B T}. \tag{10}$$

We model the interaction with the thermal bath in a relaxation-time approximation, choosing the damping matrix and damping vector so that the equation of motion (7) becomes

$$\frac{\partial}{\partial t}\vec{\lambda} = \vec{\Gamma} \times \vec{\lambda} - \frac{1}{\tau}(\vec{\lambda} - \vec{\lambda}_{ss}). \tag{11}$$

That the relaxation time τ is, in fact, an energy relaxation time can be seen by examining the energy of the cell as a function of time. The expectation value of the cell energy at any time is given by

$$E = \langle \hat{H} \rangle = \frac{\hbar}{2}\vec{\Gamma} \cdot \vec{\lambda}. \tag{12}$$

The thermal equilibrium value of the energy is

$$E_{ss} = \frac{\hbar}{2}\vec{\Gamma} \cdot \vec{\lambda}_{ss} = -\left(\frac{\hbar|\vec{\Gamma}|}{2}\right)\tanh(\Delta). \tag{13}$$

By taking the inner product of Eq. (11) with $\vec{\Gamma}$, and using Eq. (12), we obtain an equation for the time evolution of the energy,

$$\frac{d}{dt}E = \frac{d}{dt}\left(\frac{\hbar}{2}\vec{\Gamma} \cdot \vec{\lambda}\right). \tag{14}$$

If we consider the case when $\vec{\Gamma}$ is constant, i.e., neither the interdot barriers nor the neighboring polarizations are changing, then using Eq. (11) we have

$$\frac{d}{dt}E = -\frac{1}{\tau}(E - E_{ss}). \tag{15}$$

It is important to note that when the Hamiltonian, and therefore $\vec{\Gamma}$, are changing in time, both the steady-state energy E_{ss} and the steady-state coherence vector $\vec{\lambda}_{ss}$ are functions of time. Equations (11) and (15) show that, in addition to forcing terms, the coherence vector and the cell energy are each relaxing, with a time constant τ, to their instantaneous equilibrium values.

III. SINGLE CELL SWITCHING DYNAMICS

Quasi-adiabatic switching of a single cell is accomplished by applying an input signal (modeling the polarization of neighboring cells) and gradually changing the effective switching barrier. Each of these actions has the effect of changing the Hamiltonian vector $\vec{\Gamma}$, given by Eq. (5). The applied signal is the value of $\overline{P}$ and the effective switching barrier is represented by the transition energy γ. The switching event is then described by the variation in time of $\vec{\Gamma}(t)$, and the corresponding response of the system is characterized by $\vec{\lambda}(t)$, evolving under the equation of motion (11). If the switching is very slow, the coherence vector ''adiabatically follows,'' always pointing in the direction opposite to $\vec{\Gamma}(t)$, and staying arbitrarily close to the instantaneous steady-state value given by Eq. (9). A more rapid switching event causes a more complex motion, which can include exciting the system and then dissipating energy to the environment.

We consider first a single switching event in which initially the cell is in the $P=-1$ state, as is the driver, i.e., $\overline{P}=-1$. (As far as the cell dynamics is concerned, there is no distinction between the influence of electrostatic driver electrodes and the effect of neighboring cells, both simply change the value of $\overline{P}$.) The switching event shown in Fig. 3 proceeds as follows. The switching barrier is lowered (γ is raised), relaxing the cell to an essentially unpolarized state. Then the driver $\overline{P}$ changes smoothly from -1 to 1. The switching barrier is then raised (γ is lowered), repolarizing the cell in the state determined by the new value of $\overline{P}$. Each transition is smoothed by an error-function-shaped wave form in time. We evolve the system forward from the initial state by solving Eq. (11) using an implicit time-marching method. The switching event and the evolution of the cell polarization are shown in Fig. 3.

Figures 3(a)–3(d) show the time evolution for the switching event described above in the absence of any dissipation, i.e., $\tau=\infty$. Because the switching is completed in a finite time, the process is not precisely adiabatic and some energy has been transferred to the cell. This causes some excitation of the system from the ground state after the switching is complete. The cell polarization exhibits Rabi oscillations or ''ringing'' because there is no way for the extra energy to be transferred from the cell. In this case, with no coupling to the environment, the system remains in a pure superposition state and the time evolution is equivalent to that of the time-dependent Schrödinger equation.

By contrast, Figs. 3(e) and 3(f) show the same switching event when dissipation to the environment and finite temperature effects are included via Eq. (11). Here we have chosen the speed of the switching and the amount of dissipation so that the characteristic behavior is easily exhibited (clock interval $T_c = 75\,\hbar/E_k$, $T = 300\,\mathrm{K}$, and $\tau = 1000\,\hbar/E_k$). The

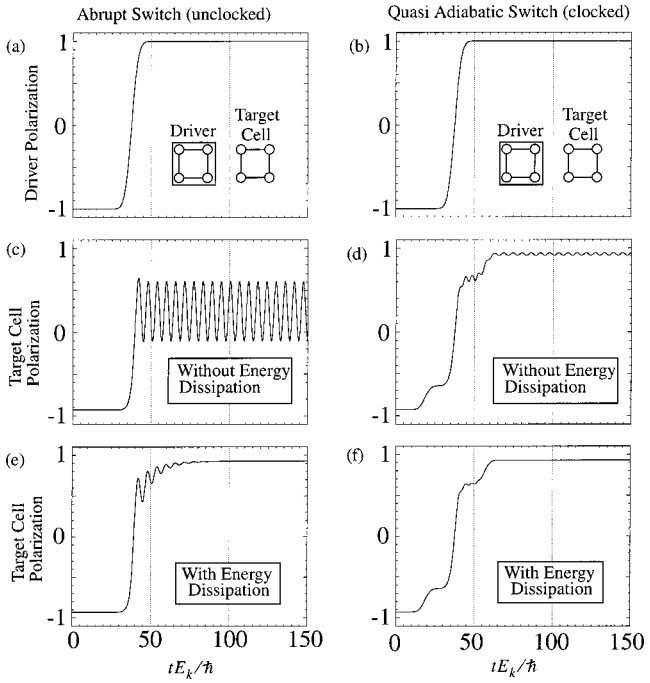

FIG. 3. Effect of quasi-adiabatic clocking and energy dissipation on cell switching response. (a) and (b) The time dependent polarization of the target cell's neighboring driver. (c) When the cell is not clocked significant ringing occurs and without dissipation it is undamped. (d) A significant portion of the ringing can be eliminated by clocking the cell, but without dissipation a slight ringing remains. (e) Without clocking a large amount of ringing is introduced; but the energy dissipation allows the cell to settle into a ground state, which corresponds to a well-defined polarization. (f) Cell switched using quasi-adiabatic clocking, with energy dissipation included through Eq. (11). The cell smoothly transitions from one ground state polarization to the next with slight temporary ringing during the switching process.

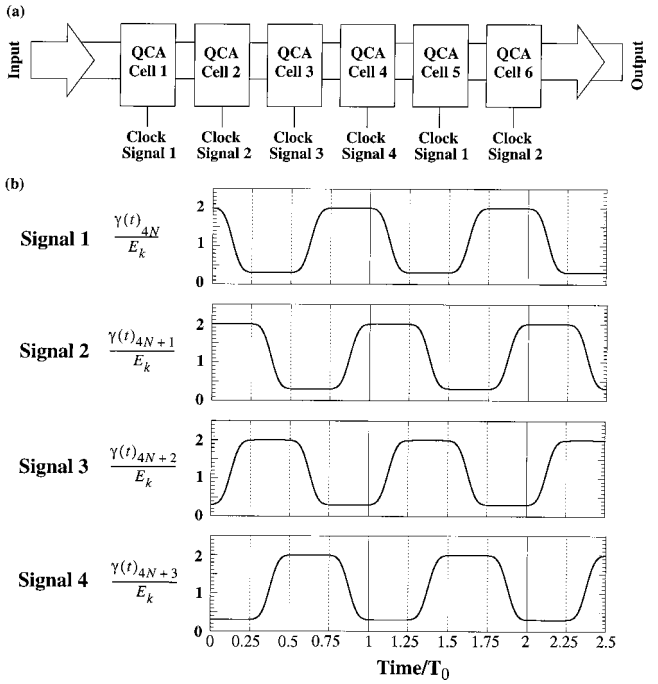

FIG. 4. (a) Schematic of a QCA shift register with a four phase clocking scheme. The data advances one cell to the right with each clock cycle. (b) The four clock signals used to produce the shift register's dynamics. The quarter period phase delay between adjacent cells facilitates the transfer of information from a locked cell to a neighboring active cell which will in turn transfer the same information to the next cell in line when it becomes locked.

Rabi oscillations are now damped by dissipative processes. The value of the formalism developed in the previous section is that we can now describe this dissipation from the system.

IV. THE QCA SHIFT REGISTER

A shift register composed of QCA cells can be formed from a linear array of cells. Adiabatic switching of such a QCA shift register was first discussed in Ref. 15, developed in detail for metal-dot cells in Ref. 16, and demonstrated experimentally for metal-dot cells in Ref. 6. The fundamental considerations of such a shift register go back to Landauer's work on fundamental limits for computation[4] and communication.[17]

To describe the action of the shift register, it is helpful to have a nomenclature which classifies the behavior of the cell according to the value of γ, the tunneling energy. (We do not concern ourselves with the detailed mechanism by which the switching barrier is raised and lowered, this is done in different ways in different implementations.[10,15,16]) When the effective switching barrier is low (γ large), we say that the cell is in the ''null'' state, holding no information. As the barrier height is increased the cell becomes ''active'' in that the polarization takes on a definite value determined by the neighboring polarizations. When the barrier height is large enough to suppress switching over the relevant time scale, we say the cell is in the ''locked'' state. The locked state may be a metastable state in which the cell polarization is independent of the environment. The locked cell is essentially a single-bit memory element.

The QCA shift register works by using the locked state of one cell as the ''driver'' input to the next cell in the register. The values of γ_j, the tunneling energy for the jth cell, are clocked using a four-phase clock with period T_c as shown in Fig. 4. During the first quarter-period, the first cell latches the input signal and locks it. Note that while that is happening, the second cell is in the ''null'' state, so that it contributes no ''back-influence.'' During the second quarter-period, the first cell is kept locked, supplying the input to the second cell which now polarizes into the same state. This copies the information from the first to the second cell. Again, during this copy operation, the downstream cell (now the third cell) is kept in the null state so that it has negligible influence over the second cell. The process continues and bit information is propagated down the line. We note that using a four phase clock, both to move information and to supply energy, is not unique to the QCA approach; Ref. 18 describes a similar clocking scheme used in RTD-HFET circuits.

In real implementations, each stage would consist of several cells; the clock signal can then be distributed using lithography on a larger length scale than individual cells. For example, molecules of nanometer dimension could be clocked by buried wires with dimensions of tens of nanometers. Moreover, as described in Ref. 15, each stage could process information, not simply copy it. For simplicity and computational tractability, we consider here only the shift register, and further assume individual clocking of cells. This

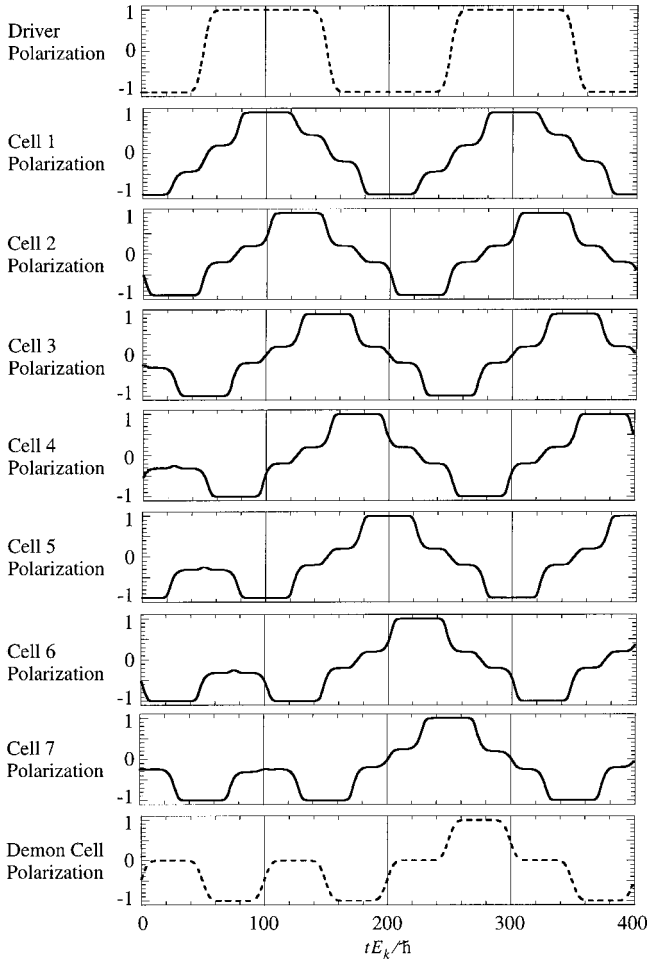

FIG. 5. Semi-infinite QCA shift register. The polarization of each cell is calculated by a self-consistent time-marching solution of Eq. (11). The initial driver polarization transition from -1 to 1 (bit value $0 \rightarrow 1$) is propagated down the cell chain, as is each succeeding driver transition. The initial polarization of the cells in the chain is -1, so the cells which are not directly adjacent to the driver retain this polarization until the initial driver pulse reaches them. The ''demon'' cell at the end of the chain simulates the response of the next cell in a semi-infinite line.

circuit, though simplified, provides a good test-bed for examining energy flow and power considerations.

Figure 5 shows the calculated polarization for a semi-infinite QCA shift register. An arbitrary bit stream can be input. Each cell is described dynamically by Eq. (11) using mean-field coupling to neighbors (and the input driver) as discussed above. The coupled system is solved forward in time using implicit time marching. For the simulation shown we have $T_c = 100\hbar/E_k$, $T = 0$ K, and $\tau = 10\hbar/E_k$. We measure times throughout in the natural units of $\hbar/E_k$.

In order to simulate a semi-infinite shift register using a finite number of cells, a special condition must be employed at the end of the array. A ''demon cell'' (after Maxwell's demon) with no physical dynamics terminates the array; it is not described by Eq. (11). Rather, the demon cell ''measures'' the polarization of the cell to its left and adopts that polarization until the cell to the left is relaxed to the null state. The demon cell thus simulates the response of a next cell in the shift register, storing a copy of the bit. The action of the demon cell and its necessity in the simulation have interesting implications for the discussion of dissipation and information erasure, which we note but will not pursue here. We use it here simply as a boundary technique which permits us to simulate a semi-infinite array with a finite array. Without it, reflections occur at the end of the cell chain and obscure the steady-state dynamics we are exploring.

This calculation, a solution of Eq. (11) for the clocked shift register, provides the basis for the analysis that follows. In the next section we examine energy flow in the shift register so that we can proceed with quantitative calculations of power gain and power dissipation.

V. POWER FLOW IN THE QCA SHIFT REGISTER

From a detailed solution of the QCA shift register, as discussed above and shown in Fig. 5, we can examine the way in which energy flows between cells, from the clock, and to the environment. The instantaneous power flow into a cell in the QCA shift register can be written [cf. Eq. (14)]

$$P^f(t) = \frac{d}{dt}E = \frac{d}{dt}\left(\frac{\hbar}{2}\vec{\Gamma}(t)\cdot\vec{\lambda}(t)\right). \tag{16}$$

The time dependence of $\vec{\lambda}(t)$ is determined, as above, by solving Eq. (11). The Hamiltonian vector for each cell is a function of time determined by both the clocking function $\gamma(t)$ and the polarization of the neighboring cells to the right and left.

$$\vec{\Gamma}(t) = \frac{1}{\hbar}\{-2\gamma(t), 0, E_k[P_L(t) + P_R(t)]\}. \tag{17}$$

We focus on the steady-state behavior of the shift register. When information is first clocked into the shift register, there are transient behaviors associated with the work being done on the array by the input. As the register is filled with information, the transients decay and the behavior becomes periodic with the clock period T_c. We examine the power flow in the shift register in this steady-state regime. The total power into the cell, averaged over a clock cycle, can be written as

$$P^f = \frac{1}{T_c}\int_t^{t+T_c} P^f(t')dt', \tag{18}$$

which in steady state becomes independent of time. Using Eq. (11), we can write this as

$$P^f = \frac{1}{T_c}\int_t^{t+T_c}\frac{\hbar}{2}\left(\frac{d\Gamma_1}{dt}\lambda_1 + \frac{d\Gamma_3}{dt}\lambda_3 - \frac{1}{\tau}[(\lambda_1\Gamma_1 + \lambda_3\Gamma_3) + \tanh(\Delta)\sqrt{(\Gamma_1)^2 + (\Gamma_3)^2}]\right)dt. \tag{19}$$

We separate the various terms in Eq. (19) to identify different components of the power flow. The net power to the bath (the environment) is

$$P_{\text{bath}} = \frac{\hbar}{2\tau T_c}\int_t^{t+T_c}\{[\lambda_1(t')\Gamma_1(t') + \lambda_3(t')\Gamma_3(t')] + \tanh[\Delta(t')]\sqrt{\Gamma_1(t')^2 + \Gamma_3(t')^2}\}dt'. \tag{20}$$

The power from the clock can be written

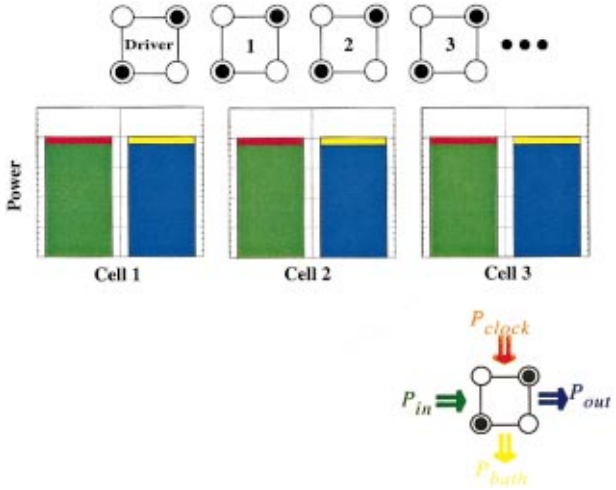

FIG. 6. (Color) Steady-state power flow in a QCA shift register. For the shift register of Fig. 5 the bar graphs show the relative magnitudes of the components of energy flow into the cell. The color code is shown below the figure. In steady state each cell has the same power profile. Energy lost to dissipative processes is restored by energy drawn from the clock. Here the power gain is unity for each cell.

$$P_{\text{clock}}=\frac{1}{T_c}\int_t^{t+T_c}\frac{\hbar}{2}\frac{d\Gamma_1(t')}{dt'}\lambda_1(t')dt'. \tag{21}$$

It should be noted that a considerable amount of energy flows into the cell from the clock as the barriers are being raised, latching the signal. Most of that energy is returned to the clock as the barriers are again lowered. By averaging over the clock period we obtain only a slight imbalance between these two flows. We do not include any energy dissipated to the environment by the clocking circuit itself. Because clocking requires only the slow (adiabatic) charging and discharging of a capacitor, the dissipation in the clocking circuit can be made arbitrarily small.

We distinguish the signal power in, from the cell to the left, and the signal power out, delivered to the cell to the right:

$$P_{\text{in}}=\frac{1}{T_c}\int_t^{t+T_c}\frac{\hbar E_k}{2}\frac{dP_L(t')}{dt'}\lambda_3(t')dt', \tag{22}$$

$$P_{\text{out}}=-\frac{1}{T_c}\int_t^{t+T_c}\frac{\hbar E_k}{2}\frac{dP_R(t')}{dt'}\lambda_3(t')dt'. \tag{23}$$

In steady state these terms, with the sign conventions we have above, sum to zero.

$$P^f=P_{\text{in}}-P_{\text{out}}+P_{\text{clock}}-P_{\text{bath}}=0. \tag{24}$$

VI. POWER GAIN IN A QCA SHIFT REGISTER

Signal power lost to the environment during a switching event can be supplied by the clock. Figure 6 shows the magnitudes of the four components of power flow into the cell [as in Eq. (24)], for a shift register in steady-state operation. The parameters have here been chosen to make the power losses evident graphically; the values used are $T_c=100\hbar/E_k$, $\tau=2\hbar/E_k$, and $T=0$ K. As evident in the figure, dissipative events cause each cell to loose some power.

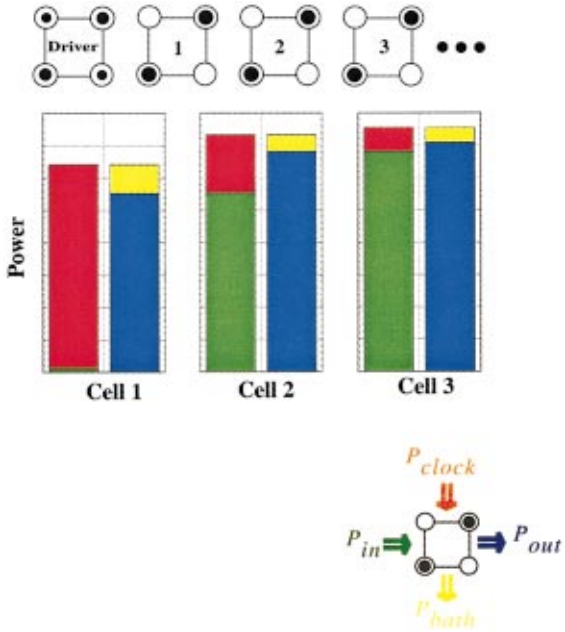

FIG. 7. (Color) Steady-state power flow in a QCA amplifier with weak input. Power flow for each cell is shown as in Fig. 6. In this case the input signal is very small, so the power from the input is augmented with power from the clock to significantly increase the power of the output signal. Each cell successively restores power to the input signal until the input signal power is equal to the output signal power.

The signal power is automatically restored by energy drawn from the clock. Physically, this occurs because the clock must do some work on a slightly unpolarized cell during the latching phase. The power gain of each cell, defined by

$$\text{gain}=\frac{P_{\text{out}}}{P_{\text{in}}}, \tag{25}$$

is in this case unity.

Power gain greater than unity occurs when the input signal is weak. Figures 7 and 8 show the power budget for each cell when the input cell polarization is very low (in this case the input polarization is ± 0.06). The first cell in the chain then sees a very small input power. The clock supplies much more power to latch the cell. The power gain of the first cell here is 46. Subsequent cells raise the signal power further, until the steady-state behavior is again recovered.

Power gain is an essential feature of an integrated electronic technology. Inevitable energy loss mechanisms must be compensated for from a power source. In conventional electronics, this is a power supply distributed by conductors to each functional element. In QCA we see that the restoring energy comes from ''hot clocks'' which though quasiadiabatic, supply the necessary restoring power.

VII. ENERGY DISSIPATION IN A QCA SHIFT REGISTER

We return to the normally operating shift register (as opposed to the case of a weak input). After the shift register has come to steady state with a continuous flow of information down the register, we monitor the power delivered to the environment through Eq. (20). Away from the input, this is independent of time and the same for all cells.

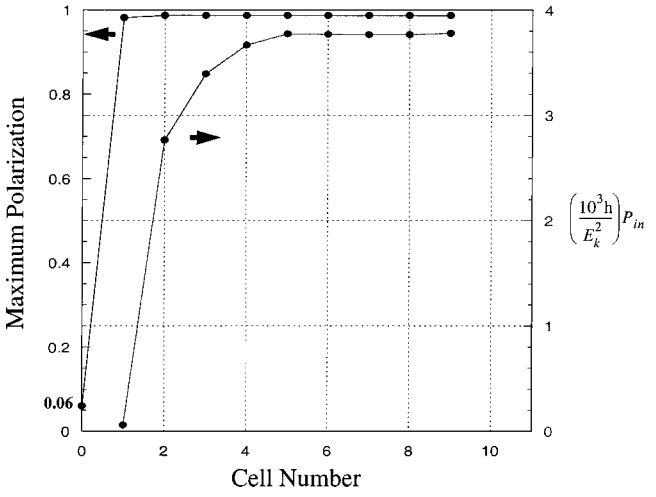

FIG. 8. Power gain in a QCA shift register. The case shown in Fig. 7 is analyzed quantitatively. The initial maximum driver polarization of 0.06 is amplified almost to 1 by the first cell. The power gain is most notable in the first cell where the power gain is approximately 46. The figure shows the restoration of the cell polarization and the corresponding restoration of the signal power.

We calculate the net power dissipation per device as a function of switching time T_c. The value of the coupling energy E_k sets the scale for the intrinsic switching time $T_0 \equiv (h/E_k)$, and of course, depends on the details of the implementation. Since we have in mind molecular implementations, where the coupling energy would likely be a few tenths of an electron volt, we choose $E_k = 100\,\text{meV}$. The value of the energy relaxation time τ also depends on the details of the implementation and how efficiently the QCA cells are coupled to the environment. We examine three cases: strong coupling for which $\tau = (\hbar/E_k)$, intermediate coupling for which $\tau = 100(\hbar/E_k)$, and weak coupling for which $\tau = 1000(\hbar/E_k)$. The results are shown in Fig. 9.

As the clock frequency increases, the power dissipated increases due to the increasing deviation from adiabatic behavior. As the period of the clock approaches T_0, (here 4.14×10^{-14} s) the deviation becomes more severe. Energy builds up in the cell and cannot be dissipated fast enough. The cell then fails, meaning that the excitation is now so great that the cell is in a very excited state and can no longer be said to be in either the ''1'' or ''0'' state. The immanent failure of the cells is signaled by the rapid increase in dissipation as the frequency is increased (the left side of Fig. 9). Note that for this value of E_k, cells do not fail until frequencies significantly exceed 1 THz.

The effect of temperature on power dissipation is also evident from Fig. 9. When the relaxation time τ is comparable to T_c, increasing the temperature from 0 to 300 K has only a very slight effect on dissipated power [Fig. 9(a)]. When $\tau \gg T_c$ increasing the temperature results in an increase in power dissipation [Fig. 11(c)].

The effects of temperature on a cell's dynamics and power dissipation can be reduced by increasing E_k. Temperature enters the equation of motion (11) only through the factor $\tanh(\Delta)$ in the expression for $\vec{\lambda}_{ss}$ [Eq. (9)]. As the value of $\tanh(\Delta)$ approaches one, $\vec{\lambda}_{ss}$ approaches the ground

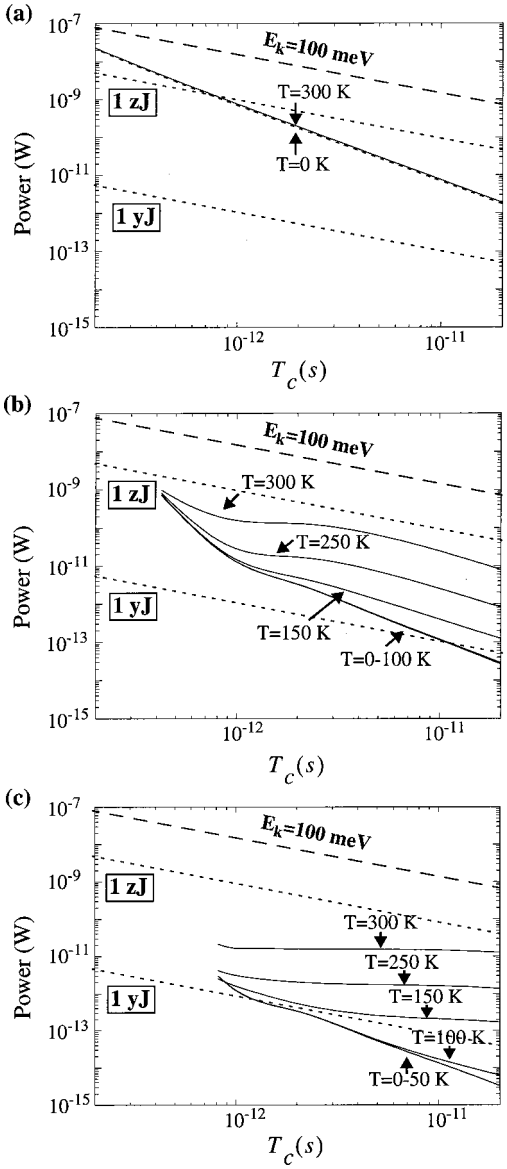

FIG. 9. The power per cell dissipated to the environment as a function of switching period. Dissipation is calculated for several values of temperature and energy relaxation time τ. (a) The case of strong coupling to the environment $\tau = 1\hbar/E_k$. (b) The case of moderate coupling $\tau = 100\hbar/E_k$. (c) The case of weak coupling to the environment $\tau = 1000\hbar/E_k$.

state coherence vector and the effect of temperature on cell dynamics becomes negligible. Figure 10 shows how quickly $\tanh(\Delta_{\min})$ diverges from unity with increasing temperature for various values of E_k where

$$\Delta_{\min} = \frac{\hbar|\vec{\Gamma}_{\min}|}{2k_B T} \approx \frac{\hbar E_k}{2k_B T}. \tag{26}$$

Note that cells with an E_k of 200 meV, still quite attainable for molecular switches, are essentially in the zero temperature limit at 300 K.

It is instructive to consider the constraints on power dissipation which attend molecular-scale integration densities (10^{11}–10^{13} devices cm^{-2}). If we take an areal dissipation of 100 W/cm^2 as an upper limit (for heat sinking), we then require an average dissipation of 10^{-9}–10^{-11} W/device.

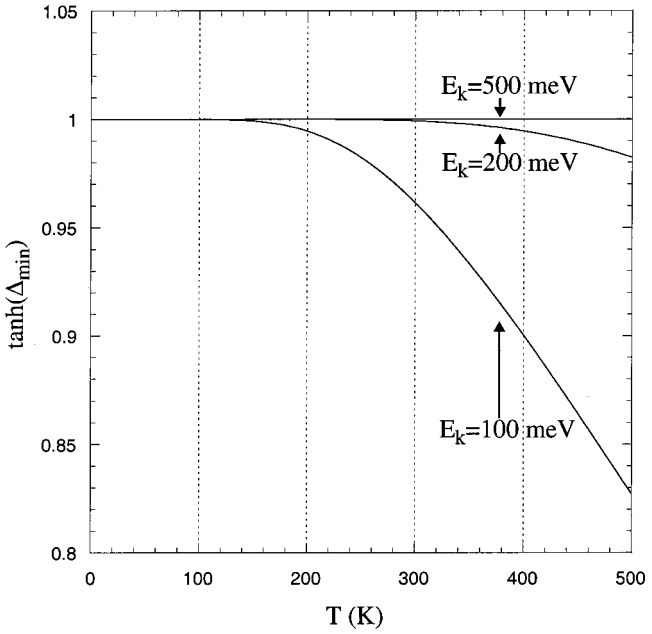

FIG. 10. Effect of temperature for various values of the cell–cell coupling energy E_k. Temperature enters the equation of motion (11) through the function $\tanh(\Delta_{min})$ where $\Delta_{min} \approx \hbar E_k / 2k_B T$. This function is shown to illustrate how higher values of E_k produce dramatically less temperature sensitivity.

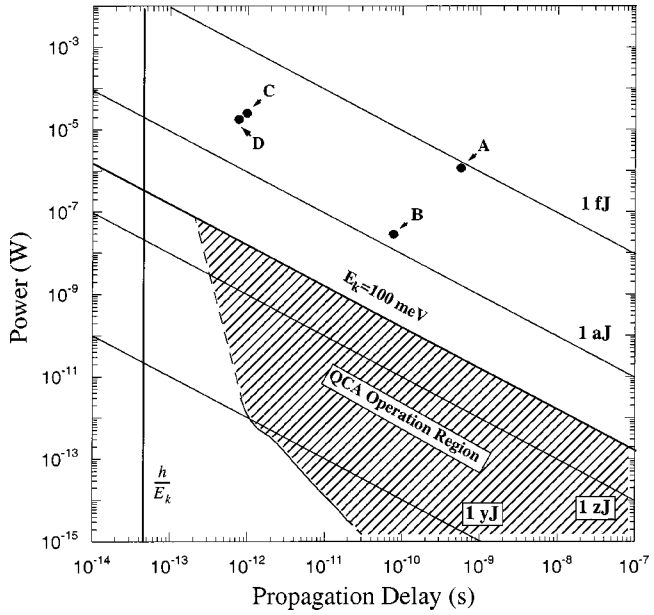

FIG. 11. Power dissipation in QCA and its relation to that of projected CMOS technology. The QCA operation region gives per device power dissipation for QCA cells as a function of switching period. The vertical line defined by h/E_k is the theoretical limit to a cell's switching speed. The upper bound on the QCA operation region corresponds to an abruptly switching cell which must dissipate the full value of its kink energy (here chosen to be 100 meV) every clock cycle. The shaded QCA operation region includes all the curves in Fig. 9. Points A and B represent the SIA road map's (Ref. 19) predictions for high-performance CMOS applications in 2001 and 2014, respectively. Points C and D correspond to the power delay properties of 30 and 20 nm gate length transistors recently fabricated at Intel Labs (Ref. 20).

Even for adiabatically switched QCA cells, this requirement limits the possible switching speed more than the intrinsic switching time does.

How does the calculated power dissipation for molecular-scale QCA compare to existing and projected technology? Figure 11 shows the power dissipated per device versus propagation delay for QCA and its relation to complementary metal–oxide–semiconductor (CMOS) technology. The upper bound for the QCA region is based on the worst-case scenario wherein every device performs a logically irreversible function and thus switches nonadiabatically, dissipating an amount of energy of order E_k during a switching period. The lower bound corresponds to the best-case scenario wherein all devices are switched quasi-adiabatically. All the curves from Fig. 9 fall in the shaded region. Actual power dissipation would depend on the fraction of cells performing logically irreversible functions and on the energy relaxation time. Points labeled A and B in Fig. 11 are based on the year 2001 and year 2014 figures from the SIA road map for semiconductors.[19] Points C and D correspond to the power-delay properties of 30 and 20 nm gate length transistors recently fabricated at Intel Labs.[20] While comparisons between proposed devices and actual devices should be made cautiously, these data support the view that QCA may offer a way to achieve the ultralow power dissipation required for molecular scales of integration.

Our examination of energy dissipated during switching does not encompass the problem of thermal noise and error correction. Both need to be addressed elsewhere. However, we can see that the present discussion does cast light on the relationship between thermal noise and power dissipation. Thermodynamically the kink energy E_k is the energy of a mistake, the excitation necessary to flip the bit into the "wrong" state. This needs to be greater than $k_B T$ in order to be able to reliably distinguish a bit value from the thermal environment [hence the oft-quoted $k_B T \log(2)$ limit]. Thermal noise effects can be improved by raising E_k (for example, by making the QCA wires two or three cells wide) and can be managed by error correction. However, what we have shown in this particular case, and Landauer showed in the general case,[4,18] is that the amount of energy dissipated during an adiabatically clocked switching event may be much less than E_k and therefore less than $k_B T$.

ACKNOWLEDGMENTS

The authors gratefully acknowledge very helpful conversations with Professor Arpad Csurgay and Geza Toth. This work was supported by the Office of Naval Research and DARPA.

[1] C. S. Lent, P. D. Tougaw, and W. Porod, Appl. Phys. Lett. **62**, 714 (1993); C. S. Lent, P. D. Tougaw, W. Porod, and G. H. Bernstein, Nanotechnology **4**, 49 (1993).
[2] The QCA concept can be extended to the quantum-computing regime. See G. Toth and C. S. Lent, Phys. Rev. A **63**, 052315 (2001).
[3] P. D. Tougaw and C. S. Lent, J. Appl. Phys. **75**, 1818 (1994).
[4] R. Landauer and R. W. Keyes, IBM J. Res. Dev. **14**, 152 (1970).
[5] C. S. Lent and P. D. Tougaw, J. Appl. Phys. **75**, 4077 (1994); G. Toth and C. S. Lent, *ibid.* **85**, 2977 (1999); A. O. Orlov, I. Amlani, G. H. Bernstein, C. S. Lent, and G. L. Snider, Science **277**, 928 (1997); I. Amlani, A. Orlov, G. Toth, G. H. Bernstein, C. S. Lent, G. L. Snider, *ibid.* **284**, 289 (1999).
[6] A. O. Orlov, I. Amlani, R. Kummamuru, R. Rajagopal, G. Toth, C. S. Lent, G. H. Bernstein, and G. L. Snider, Appl. Phys. Lett. **77**, 295 (2000); A. O. Orlov, R. Kummamuru, R. Ramasubramaniam, G. Toth, C. S. Lent,

G. H. Bernstein and G. L. Snider, *ibid.* (to be published).
[7] M. Niemier and P. M. Kogge, in International Conference on Electronics, Circuits and Systems (ICECS '99), Cyprus, 1999.
[8] C. S. Lent, Science **288**, 1597 (2000).
[9] M. Lieberman, S. Chellamma, B. Varughese, Y. Wang, C. S. Lent, G. H. Bernstein, G. L. Snider, and F. C. Peiris, in Proceedings of the Conference on Molecular Electronics, Hilo, 2000 (to be published).
[10] K. Hennessy and C. S. Lent, J. Vac. Sci. Technol. B **17**, 1752 (2001).
[11] D. J. Griffiths, *Introduction to Quantum Mechanics* (Prentice-Hall, Englewood Cliffs, NJ, 1994).
[12] We use the sign convention for the Pauli matrices of Ref. 13.
[13] P. D. Tougaw and C. S. Lent, J. Appl. Phys. **80**, 4722 (1996).
[14] G. Mahler and V. A. Weberruß, *Quantum Networks: Dynamics of Open Nanostructures* (Springer, New York, 1995).
[15] C. S. Lent and P. D. Tougaw, Proc. IEEE **85**, 541 (1997).
[16] G. Toth and C. S. Lent, J. Appl. Phys. **85**, 2977 (1999).
[17] R. Landauer, Appl. Phys. Lett. **51**, 2056 (1987).
[18] C. Pacha, U. Auer, C. Burwick, P. Glosekotter, A. Brennemann, W. Prost, F.-J. Tegude, and K. F. Goser, IEEE Trans. VLSI **8**, 558 (2000).
[19] SIA road map (revision 2000). In 2001 CMOS technology for high performance applications will have the following characteristics: on chip local clock frequencies will attain 1.77 GHz, there will be 122 million transistors on a chip, and a chip will dissipate 130 W of power. These characteristics combine to give an average device power of 1.07 μW/transistor and a device switching energy of 0.6 fJ. The predictions for high-performance CMOS applications in the year 2014 include on chip local clock frequencies of 13.5 GHz, 11 052 million transistors on a chip, and a chip will dissipate 186 W of power. These characteristics combine to give an average device power of 16.8 nW/transistor and a device switching energy of 1.25 aJ.
[20] R. Chau and G. Marcyk, "Intel establishes new transistor performance record," available at: http://www.intel.com/research/silicon/micron.htm, June 2001.